Snow depth, density, and SWE estimates derived from GPS reflection data: Validation in the western U.S.

James L. McCreight

Department of Aerospace Engineering Sciences, University of Colorado, Boulder, CO, USA.

Eric E. Small

Department of Geological Sciences, University of Colorado, Boulder, CO, USA.

Kristine M. Larson

Department of Aerospace Engineering Sciences, University of Colorado, Boulder, CO, USA.

Corresponding Author:

James L. McCreight, Aerospace Engineering Sciences, Campus Box 399, University of Colorado, Boulder, CO 80309, USA. (mccreigh@gmail.com)

Key Points

- GPS-based snow depth measurements validated at 18 sites near peak snow accumulation
- Snow water equivalent calculated from snow density modeled on GPS-based depth observations
- Near real-time, GPS-based snow depth and SWE are accurate enough for most applications

Abstract

Geodetic-quality GPS systems can be used to measure average snow depth in the ~1000 m^2 area around the GPS antenna, a sensing footprint size intermediate between *in situ* and satellite observations. SWE can be calculated from density estimates modeled on the GPS-based snow depth time series. We assess the accuracy of GPS-based snow depth, density, and SWE data at 18 GPS sites via comparison to manual observations. The manual validation survey was completed around the time of peak accumulation at each site. Daily snow depth derived from GPS reflection data is very similar to the mean snow depth measured manually in the ~1000 m^2 scale area around each antenna. This comparison spans site-averaged depths from 0 to 150 cm. The GPS depth data exhibit a small negative bias (-6 cm) across this range of snow depths. Errors tend to be smaller at sites with more usable GPS ground tracks. Snow bulk density is modeled using the GPS snow depth time series and model parameters are estimated from nearby SNOTEL sites. Modeled density is within 0.02 $g*cm^{-3}$ of the density measured in a single snow pit at the validation sites, for 12 of 18 comparisons. GPS-based depth and modeled density are multiplied to estimate SWE. SWE estimates are very accurate over the range observed at the validation sites, from 0 to 60 cm (R^2 = 0.97 and bias = -2 cm). These results show that the near real-time GPS snow products have errors small enough for most applications.

Index Terms:

Snow, Remote sensing, Instruments and techniques, Modeling

48 **1. Introduction**

49 Snow is an important environmental variable. It governs energy and water fluxes, influencing
50 both weather and climate (e.g. *Walsh* [1984], *Cohen and Entekhabi* [2001]). Snow is also the
51 primary water resource in many areas of the world [*Beniston*, 2003]. Snow depth, snow density,
52 and snow water equivalent (SWE) are fundamental characteristics of seasonal snow packs. SWE
53 is the liquid depth of melted snow, and thus is critically important for water resources
54 management. SWE is difficult and time-consuming to measure [*Sturm et al.*, 2010]. Snow depth
55 is much easier to measure, but it only yields useful information about water storage when
56 combined with measurements or estimates of snow density. Recently, a method has been
57 developed to measure snow depth using networks of geodetic-quality GPS instruments [*Larson*
58 *et al.*, 2009]. This method has been applied to GPS data collected in the western United States
59 (Figure 1), producing snow depth time series that can augment existing snow networks [*Larson*
60 *and Nievinski*, 2013]. The majority of the GPS sites in this new snow database are part of NSF's
61 Plate Boundary Observatory (PBO), and thus the GPS snow network is referred to as the PBO
62 H2O project (http://xenon.colorado.edu/portal). A model was also developed to estimate density
63 from these GPS-based snow depth time series [*McCreight and Small*, 2014], allowing for
64 calculations of SWE. In this paper, we assess the accuracy of GPS-based snow depth, density,
65 and SWE data generated at PBO H2O sites, via comparison to manual observations at 18 sites in
66 the Rocky Mountains.

67 Snow depth, bulk density, and SWE can be measured on the ground. The simplest snow depth
68 measurement is by manual snow probe (e.g. *Sturm* [2009]). Similarly, fixed probes have been
69 placed in view of time-lapse cameras to automate the measurement (e.g. *Garvleman et al.*
70 [2013]). Ultrasonic snow depth sensors also provide automated measurements, including at an

71 increasing number of SNOTEL sites [*Serreze et al.*, 1999]. The spatial footprint of an ultrasonic
72 sensor is ~1 m^2 [*Ryan et al.*, 2008]. Snow depth can be converted to SWE whenever snow bulk
73 density is measured. Bulk density is a labor-intensive measurement that requires digging and
74 sampling a snow pit (e.g. *Dixon and Boon* [2012]). However, SWE can be directly measured
75 using SWE tubes, such as a federal sampler (e.g. *Farnes et al.* [1982]), as done for snow courses
76 performed by various water districts in the US and Canada [*Cyan*, 1996; *Goodison et al.,* 1987].
77 The sampling footprint of these ground measurements is very small, much less than a square
78 meter. To obtain representative SWE values in the presence of spatial variability, intensive labor
79 is often required (e.g. snow courses). Automated measurements of SWE, found primarily on the
80 SNOTEL network, are performed by pressure sensors with spatial footprints of approximately 3
81 m^2 [*Johnson et al.*, 2007]. Most automated measurements of depth and SWE provide no
82 characterization of local variability in either property. In addition, these measurements do not
83 represent a wide area. Recently, ground-based LiDAR has transformed the ability to measure
84 snow depth over large areas with high accuracy, but these systems remain expensive, are rarely
85 automated, and require bare-earth measurements of terrain elevations (e.g. *Gutmann et al.*
86 [2012]).

87 Satellite and airborne remote sensing techniques have been used to estimate snow covered area
88 (SCA), snow depth, and SWE. Compared to ground-based measurements, satellite estimates
89 generally offer greater continuity in both space and time. Optical data is useful for retrieving
90 SCA at a moderate resolution [*Painter et al.*, 2009; *Rittger et al.*, 2013]. However, cloud cover
91 poses difficulties. Airborne LiDAR provides high-resolution snow depth measurements, though
92 overflights are typically infrequent if repeated at all [*Harpold et al.*, 2014]. Snow depth and SWE
93 are estimated using both passive and active microwave approaches. Microwave retrievals are

problematic in many locations. The spatial footprint of passive techniques is very large compared to snow variations. Both microwave approaches remain inaccurate because of uncertainties in snow grain size as well as surface and subsurface snow properties [*Dietz et al.*, 2012]. Remote sensing approaches have not provided reliable estimates of snow depth or SWE which are continuous through time.

Larson et al. [2009] first showed that geodetic-quality GPS systems (Figure 2) can be used to measure snow depth. The approach uses active microwave reflectometry in a bistatic geometry (Figure 3), rather than the monostatic geometry typical of satellite remote sensing. This geometry makes the snow depth measurement local to the receiving antenna. Snow depth estimates from usable GPS ground tracks can be combined, yielding a sampling footprint around the antenna of ~1,000 m^2. This footprint is much larger than that of *in situ* snow depth measurements but smaller than satellite microwave measurements. Snow depth estimates from these GPS sites could be used to augment existing snow observation networks, particularly if the GPS-based depth estimates were converted to SWE based on information about snow density.

Previous studies of the accuracy of GPS snow depth measurements were fairly limited in scope. *Larson et al.* [2009] analyzed measurements from two spring snowstorms at an ephemeral snow site near Boulder, Colorado. They showed strong agreement between GPS snow depth estimates, field measurements, and nearby ultrasonic snow depth measurements. *Gutmann et al.* [2012] compared GPS data from an alpine site (Niwot Ridge) to terrestrial LiDAR scans and pole measurements. At peak accumulation, they reported an RMSE of 13 cm between LiDAR and GPS. During the melt phase, these errors were slightly smaller. However, the footprints of the LiDAR and GPS systems did not fully coincide and the site had extremely high spatial variability in snow depth. Finally, *Nievinski and Larson* [2014a] compared GPS snow depth

117 retrievals with single snow pole depth observations over multiple years at two sites and manual
118 depth surveys at a third site in a single year. They found a high-correlation (> 0.97) between the
119 GPS and *in situ* measurements, but stronger conclusions were hampered by the fact that the
120 footprints of the manual and GPS measurements were dissimilar in scale.

121 Here, we assess the accuracy of GPS-based snow depth measurements at GPS sites via
122 comparison to extensive field observations. Additionally, we evaluate snow density and SWE
123 estimates that are based on the GPS snow depth time series. Thus this paper expands upon the
124 previous studies of GPS-based snow depth in three ways. First, we compare GPS snow depth to
125 manual observations at equivalent spatial scales. All of the previous GPS snow depth validation
126 was based on comparisons to depth measured at a point, with the exception of one site used by
127 *Nievinski and Larson* [2014b]. Here, the GPS snow depths are compared to manual depth
128 measurements throughout each ~1000 m^2 GPS sensing footprint. Second, we compare manual
129 snow observations and GPS-based snow products at 18 GPS sites in five western U.S states,
130 greatly expanding the range of conditions for which the GPS snow products are evaluated. Third,
131 we compare the GPS-based snow density and SWE products to observations. This is the first test
132 of the *McCreight and Small* [2014] density model applied to GPS sites. Comparisons between
133 GPS snow products and manual observations focus on the 2 week period near peak snow
134 accumulation, the time most relevant to water management.

135 The outline of this paper is as follows. The methods section includes a description of: (1) the
136 GPS data and how it is analyzed to estimate snow depth; (2) the manual snow depth and density
137 observations used for comparison to the GPS snow products; and (3) the model used to estimate
138 density and SWE from the GPS-based snow depth time series. In the results, we first compare
139 GPS snow products and manual observations from 18 sites at peak snow accumulation, yielding

140 error estimates for the GPS snow products. Then, season-long observations from three sites are
141 used to put the peak accumulation analysis in the context of seasonal accumulation and melt. In
142 the discussion, we describe sources of error, evaluate the representativeness of the validation
143 sites, and identify uses for and constraints on existing and future GPS-based snow products.

144 **2. Methods**

145 ***2.1. GPS snow depth measurement.***

146 The GPS snow depth method used by PBO H2O is described in detail by *Larson and Nievinski*
147 [2013], so here only a brief summary is given. The method uses reflected signals that are
148 transmitted by satellites in the GPS constellation. GPS signals are L-band, with wavelengths of
149 19 and 24.4 cm on the primary frequencies. The Signal to Noise Ratio (SNR) observable
150 recorded by GPS instruments is sensitive to the interference between the direct signal (used by
151 geophysicists and surveyors) and the reflected signal (Figure 3). As a satellite rises (or sets), the
152 extra path length traveled by the reflected signal changes. This means that the interference
153 pattern will change depending on the elevation angle of the satellite, the signal wavelength, and
154 the height of the GPS antenna above the reflecting surface. The latter quantity, the GPS reflector
155 height, is estimated from the GPS SNR data using a Lomb Scargle Periodogram [*Press et al.*,
156 1996]. By comparing the reflector heights estimated from snow surfaces to reflector heights
157 estimated from late fall (typically an average for 30 days), when bare soil conditions are
158 prevalent, snow depth can be determined.

159 A GPS ground track is the path along the surface traced by the specular point of the reflected
160 signal from an individual GPS satellite. The specular point moves towards the antenna as the
161 elevation angle increases. The reflection geometry of ground tracks observed by a GPS antenna
162 depends on its height above the surface. More generally, the satellite geometry depends on the

latitude of the GPS receiver and the inclination of the GPS satellites (55 degrees). This results in no satellite tracks between azimuths of ~315-45 degrees in the Rocky Mountain region. In the southern hemisphere, this situation is reversed. Sample reflection (first Fresnel) zones from different satellites are shown for a GPS site in Figure 4. These areas are long ellipses, ~25 meters long and ~5 meters across for a satellite elevation angle of 10 degrees. The Fresnel zone shown is representative of the average Fresnel zone for the full pass used to derive snow depth, which in this study was for 5 to 30 degrees. The average sampling footprint given for the GPS method is based on the length of these reflection zones (~25 m) for all visible satellites, which is a region ~1000 m^2 around a GPS antenna that is 2 meters above the reflection surface. One complexity of the GPS snow method is that when a significant amount of snow is on the ground, the Fresnel zones are smaller and closer to the antenna, i.e. the reflection region is smaller. We approximate the radius, r, of the reflection area as a function of snow depth, h_{snow}, using the following equation:

$$r = 21 - 5 * h_{\mathrm{snow}} \quad \text{(Eq. 1)}$$

where r and h_{snow} are both in meters. When the snow surface is ~0.5 m or closer to the antenna, snow depth cannot be estimated from the GPS data, and this equation does not apply.

The daily snow depth value used in this paper is an average for all snow depths available for individual satellite ground tracks on a given day (UTC time). The number of available ground tracks on the day of the manual snow survey varies from 1 to 12 across the sites (Table 1). The standard deviation over the snow depths of individual GPS ground tracks which produced measurable estimates of snow depth is combined in quadrature with an uncertainty based on bare soil reflections to provide an error estimate, or standard deviation, on the mean snow depth

185 value. This error is not a true measurement error because it encompasses variability in snow
186 depth around the antenna. We know the GPS method fails if the snow level becomes too close to
187 the antenna. Simulations show that the snow surface should be ~50 cm (two wavelengths) from
188 the antenna [*Nievinski and Larson*, 2014a]. Readers with an interest in how the quality of the
189 reflector height retrievals are assessed are directed to *Larson and Nievinski* [2013].

190 The PBO H2O group currently estimates snow depth for 130 sites. Twenty-five sites are in
191 Alaska; the remaining sites are primarily located in the western US: Idaho, Montana, Wyoming,
192 Oregon, Washington, Colorado, Utah, California and Nevada (Figure 1). With two exceptions,
193 these sites were installed to measure position, either by geophysicists (PBO) or to support
194 surveyors. This means that the antennas were placed to ensure visibility to the direct GPS signals
195 so that positioning precision could be optimized. This also means that no GPS sites are located
196 within heavily forested regions. The location of GPS sites installed by geophysicists for the Plate
197 Boundary Observatory were dictated by geologic features, and thus are often found far from
198 urban areas. GPS sites installed by surveyors are installed in both urban and rural areas.

199 ***2.2 In situ observations***

200 We selected 18 PBO H2O snow sites in Colorado, Utah, Wyoming, Montana, and Idaho to
201 validate (Figure 1, Table 1) during the manual survey. These sites were chosen based on three
202 criteria. First, the sites were located along a relatively direct route, allowing for one or two site
203 visits per sampling day. Second, the validation sites needed to be representative of the entire
204 population of PBO H2O snow sites in terms of the number of usable ground tracks. Third, we
205 needed access to the site for sampling. Some GPS sites in the network are practically
206 inaccessible during the winter, requiring more than a day of backcountry travel from the nearest
207 road. Other sites were excluded due to land-owner constraints.

208 The following sampling procedures were followed at each site. Snow depth was measured every
209 meter along 6 transects, each extending from the antenna to a distance of 25 m. This distance
210 was selected based on the sensing footprint for a standard height (2 m) GPS antenna (Figure 4).
211 Snow depth was measured via snow probe and depth was recorded to the nearest centimeter. In
212 the absence of snow at any sampling location, a zero depth was recorded. Transect azimuths
213 were the same at all sites (Figure 4). Azimuths were chosen to evaluate if GPS measures a
214 representative average snow depth over the 1000 m^2 around the antenna. Therefore, three
215 transects were located to the north of the antenna and three to the south, even though most GPS
216 tracks are to the south of the antenna (in the northern hemisphere). At most sites, this protocol
217 yielded 150 measurements of snow depth. At several sites, topographic constraints (e.g., a cliff)
218 or vegetation precluded measurements of depth at some planned sampling locations, yielding
219 fewer total measurements.

220 Density was measured at a single snow pit in the GPS footprint. Pits were located ~10 m to the
221 southeast or southwest of each antenna, with the exact location depending upon site access and
222 location of infrastructure (e.g., solar panels, cattle fences, etc.). A 1000 mL snow cutter was
223 inserted into the face of the pit at 10 cm intervals from the snow surface to the ground. The mass
224 of snow was measured and density calculated from the known volume excavated (e.g. *Elder et*
225 *al.* [1991]). Density was measured after snow depth. This allowed us to dig the snow pits in
226 locations with snow depth typical of each site. Modeled snow densities are compared to the
227 single observed pit value at each site.

228 In the results section, we assess if GPS-based SWE represents the average SWE in the GPS
229 footprint. We calculate observed, areal-average SWE as the product of the single density
230 measurement and the average snow depth found by probing the footprint. We acknowledge that

231 this calculation is only an approximation because of potential spatial variability in density and its
232 nonlinear dependence on snow depth, particularly for snow depths above 80 cm [*Pomeroy and*
233 *Gray*, 1995; *Sturm et al.*, 2010]. However, this approximation is reasonable and often made in
234 practice due to the difficulty of measuring snow density spatially and because density varies
235 much less than snow depth over the same area [*Dickinson and Whitely*, 1972; *Stepphun and*
236 *Dyck*, 1974; *Marchand and Killingtveit*, 2004; *Elder et al.*, 1991]. The only location which
237 challenges this assumption in our study is P455, which exhibited extreme spatial variability in
238 snow depth.

239 Seventeen of the sites were visited once during February or March of 2012, within
240 approximately 1 week of observed peak accumulation at each site. One site of these sites (P029)
241 was revisited in 2013, again near the time of peak accumulation. The RN86 site was visited 6
242 times in both the 2012 and 2013 water years. Density and SWE were measured during five of the
243 six visits in each year. Our main validation data set consists of 20 total observations at 18 distinct
244 locations made around the time of peak accumulation (Figure 1; Table 1). We include all
245 seventeen observations from 2012, the observation at P029 in 2013, and the observations at
246 RN86 in each year with the largest snow depth. Only 16 of these depth observations have
247 associated density observations as three locations had no snow and it was not possible to
248 measure density at one location. Though manual observations were collected at p351, no GPS
249 data were available within a week of these. From the earlier GPS observations it could be
250 inferred that snow had encroached on the antenna and the manual observation confirmed
251 this. Therefore, the data from p351 (Table 1) are not included in the analysis.

252 After validation of estimates at peak-accumulation, additional time series data from three sites
253 are analyzed to examine the suitability of GPS for measuring seasonal snow accumulation and

254 melt. Time-lapse photography was used at two sites (P360 and P101) to provide depth estimates
255 at single points within their GPS footprints. A fixed snow pole was photographed every three
256 hours, and these observations were averaged to a single daily depth value. The twelve manual
257 surveys at RN86 are also used to assess the seasonal progression of accumulation and melt.

258 ***2.3 Density model and SWE***

259 The GPS method provides estimates of snow depth, but information about SWE is needed for
260 many applications. Given snow depth, snow bulk density can be used to calculate SWE. Snow
261 bulk density varies within a narrow range and can be estimated based on snow depth and other
262 predictors [*Jonas et al.*, 2009; *Sturm et al.*, 2010]. In contrast, snow depth varies greatly. Snow
263 depth is therefore the more important factor in determining SWE. For this reason, errors in
264 modeled density have a limited effect on SWE errors when depth is observed. For example, the
265 model of *McCreight and Small* [2014] explained only 56% of the observed variance in density
266 throughout the snow season and 71% of the variance near peak-accumulation, which was greater
267 than the other models considered in their study. Though the density model was not very accurate,
268 96% of the observed SWE variance was explained when modeled densities were multiplied by
269 known snow depths, both for the full snow season and near peak accumulation. This
270 demonstrates that even if the density model is imperfect, useful SWE estimates can be obtained
271 if GPS-measured snow depth is accurate.

272 The *McCreight and Small* [2014] bulk density model, illustrated in Figure 5, was developed to
273 transform daily snow depth observations to SWE. The model recognizes that snow depth and
274 bulk density are negatively correlated at short (10 days) timescales while positively correlated at
275 longer (90 days) timescales. Previous models focused on longer timescales while neglecting how
276 daily snow accumulation and ablation tend to decrease and increase bulk density, respectively.

McCreight and Small [2014] modeled density over both short and long timescales by separating observed snow depth time series into three components, used as predictors of density in a linear regression model. The long-timescale variability is modeled using a running average snow depth, *hAvg*, computed on a window of 21 days (second panel of Figure 5). Anomalies from this average model the short-timescale variability and are separated into two different predictors by sign, *hAbove* and *hBelow* (third panel of Figure 5). A fourth predictor is a daily climatology of fit, ρ_{Clim} (fourth panel of Figure 5).

The regression model is given by the following equation:

$$\rho(h, month, neighbors) = a * hAvg + b * hAbove + c * hBelow + d * \rho_{clim} + e \quad \text{(Eq. 2)}$$

Application of this model to a GPS site, where density is not observed, requires solving the model parameters using observations of the relationship between depth and density. We solve these parameters for each PBO H2O site separately on a monthly basis, using collocated depth and density data from SNOTEL sites within 70 km of the GPS site. There are between 3 and 34 SNOTEL sites within 70 km of each PBO H2O site. At each site observed snow depth, *h*, from each SNOTEL is split into the three new predictors described above. The ρ_{Clim} predictor for each GPS site is calculated as the average observed density on each day of the year over the set of neighboring SNOTEL sites. Ordinary least squares is used to solve for the model parameters against the observed densities. At each GPS site, density is then modeled using the GPS-observed snow depths, the five parameters estimated for that site, and the density climatology. Finally, SWE is calculated as the product of modeled density and observed depth.

296 Uncertainty in modeled density (e.g., error bars in Figure 5, panel 5) at a GPS site is estimated by
297 treating each SNOTEL site used for training as if it were a GPS site and characterizing the set of
298 density errors resulting from this leave-one-out cross validation. Following the model fitting
299 procedure above, each SNOTEL site is withheld in-turn from the parameter fitting process. Its
300 observed densities are then estimated from its observed snow depths using the parameters and
301 climatology derived from the remaining SNOTEL sites. This yields a set of density errors
302 (modeled-observed) that result from model structural errors and from parameter transfer to a
303 location where density is not observed. For each day of year, the standard deviation of these
304 errors describes the uncertainty in the model estimate at the GPS site. For example, there are 34
305 SNOTEL sites within 70 km of P118. At each of these SNOTEL sites, the time series of
306 observed densities is estimated using parameters and the climatology based on the remaining 33
307 SNOTEL sites while using its own observed snow depths for the predictor variables. The density
308 errors over all water years at all 34 SNOTEL sites are then collected by day of year. The
309 standard deviation of these errors on each day of year describes the uncertainty in density
310 estimation for the GPS site on that day.

311 Uncertainty described by this cross-validation process includes error resulting from parameter
312 transfer between SNOTEL sites. Parameter transfer between SNOTEL sites contributed 2.6 cm
313 to SWE RMSE scores at a site [*McCreight and Small*, 2014]. Physiographic differences between
314 SNOTEL and GPS sites are greater than between SNOTEL sites, which could mean larger errors
315 from parameter transfer. GPS sites tend to be at lower elevations than the SNOTEL sites within
316 70 km that are used for estimating parameters. In addition, GPS sites are located in large
317 clearings or non-forested areas, whereas SNOTEL are mostly located amidst forests. This leads
318 to differences in exposure to wind and radiation (both long wave and solar). As a result,

319 uncertainty in density estimates may be underestimated for PBO H2O sites. Our calculated
320 uncertainty in SWE combines the uncertainties in modeled density and in GPS-observed snow
321 depth. SWE standard deviations are calculated for each day of year as the vector sum of the
322 (assumed) independent depth and density standard deviations.

323 Interpreting the spatial scale represented by modeled density and SWE is not straightforward.
324 Though we validate against point density measurements and estimates of areal average SWE, we
325 can claim only that these modeled quantities represent the best possible estimates based on
326 available data. Likewise, error estimates for modeled density and SWE represent a best attempt
327 at quantifying their uncertainty.

328 **3. Results**

329 ***3.1 Peak SWE observations***

330 Snow depth and SWE were relatively low in many parts of the western U.S. during the 2012
331 snow year. Depending on location, depth and SWE in 2012 were as much as 50% below normal.
332 Three sites (P030, P353, P684) had no snow at the time of the 2012 survey (Table 1). In most
333 years, maximum snow depth at P030 and P684 is more than 0.5 m. Snow is ephemeral at P353
334 and rarely exceeds 10 cm. We include data from these three sites in our comparison.

335 ***3.1.1 Snow depth***

336 At each site, the mean GPS snow depth closely matches the mean depth measured *in situ* (Figure
337 6, top panel). This indicates that site-average GPS depth estimates provide a reliable measure of
338 snow depth within a 25 m radius of the antenna, or at the ~1000 m^2 scale. The depth comparison
339 spans a broad range, from no snow to 150 cm, with GPS explaining 96% (=R^2) of the observed
340 variance. There is a small negative bias (-5.7 cm) that is consistent across the range of snow
341 depth. The RMSE between GPS and *in situ* depth is 10.3 cm. When the bias is removed, RMSE

342 decreases to 8.7 cm. As discussed above, three sites had no snow or very little snow during the
343 2012 survey. At these sites, the GPS depth measurements match the observed, zero snow depths.
344 Summary statistics are effectively the same when observations from these snow-free sites are
345 excluded from the comparison (Table 2).

346 The number of GPS ground tracks that yield usable data varies between sites and through time.
347 On the days that *in situ* data were collected, the number of ground tracks used at each site varies
348 from one (P682) to twelve (P360) (Table 1). The symbols used in Figure 6 indicate the number
349 of GPS tracks used to calculate the GPS mean snow depth on the day of the manual observation.
350 The largest differences between GPS and mean *in situ* depth are at P676 and P682, where only
351 three and one tracks (respectively) were used to calculate the site-average GPS depth. Site-
352 average GPS depths were based on less than four tracks at only two other sites. When data from
353 these four sites are excluded, the bias is reduced to only -3.2 cm and RMSE to 6.6 cm (unbiased
354 RMSE to 5.8 cm). This result is expected: when more ground tracks are used to calculate the site
355 average, the correspondence with average snow depth measured *in situ* should be closer. This is
356 especially true at sites with significant snow depth variability over the GPS footprint.

357 Figure 6 (top) compares the mean GPS snow depth at each site with the corresponding mean of
358 all *in situ* observations within 25 m of the antenna. However, the length of each GPS ground
359 track on a given day depends on the antenna height above the reflecting surface: as snow depth
360 increases, the reflection area decreases (section 2.1). We recalculate the statistics to compare the
361 mean GPS depth with the mean of the *in situ* observations falling within the depth-dependent
362 ground track radius (equation 1). The mean *in situ* snow depth is used to estimate the ground
363 track length at each GPS antenna. For example, at sites with ~150 cm of snow, the average *in*
364 *situ* observation only includes data within ~10 m of the antenna. Table 2 summarizes the

validation statistics considering the fixed, snow-free footprint (~20 m radius) and the footprint that varies as a function of snow depth. The statistics are nearly identical regardless of which subset of *in situ* data is used. Statistics based on depth-dependent track length excluding the three snow-free observations are also very similar.

3.1.2 Snow depth variability and GPS accuracy

We observed a wide range of snow depth variability within the sensing zone at the validation sites. Table 1 shows both (1) the standard deviation of the 150 manual points at each site, varying from 4.6 to 33.5 cm; and (2) the standard deviation of the six manual transect mean values at each site, varying from 1.0 to 32.6 cm. The vertical error bars in Figure 6 (top) represent the latter value. These can be more directly compared to variability of depth estimates calculated over individual GPS ground tracks. Sites P676, P682, and P455 had the greatest snow depth variability. Their manual point measurements ranged over 91 cm and their standard deviations ranged from 19-34 cm (Table 1). The greatest variability between manual transects was observed at P676 and P455. Amongst these three sites, P455 had the greatest snow depth variability. Roughly 20% of the sampled area had no snow, whereas snow depth exceeded one meter along a 6m portion of the transect to the northwest of the antenna. The remainder of the sites showed much less spatial variability (Table 1).

There is a potential for large differences between the GPS depth and the mean *in situ* snow depth at sites where there are few usable GPS ground tracks and snow depth is variable. The usable GPS ground tracks may be located in parts of the GPS footprint that have snow depth well above or below the mean. The two greatest GPS snow depth errors occur at sites with high variability and few usable ground tracks. Site P676 has the largest absolute GPS snow depth error. At this site, there were only three usable ground tracks, which were clustered within 50 degrees of

azimuth. As a result, the GPS depth estimate represents only ~15% of the 1000 m^2 area around the antenna. Comparison of the manual transect that is closest to the three usable GPS tracks yields a bias of -10 cm, instead of -31.3 cm. Significant snow depth variability was also observed at site P682 where only one GPS track was available on the day of observation. This site had the second largest (-18 cm) error. P455 had the smallest absolute error (2.5 cm) of the sites with greatest spatial variability, probably because the five usable GPS tracks were distributed across the GPS footprint.

We now evaluate if the inter-track variability at a site provides an accurate measure of snow depth spatial variability within the GPS footprint. The following two measures of variability are compared: (1) the standard deviation of the depths estimated from the individual GPS tracks and (2) the standard deviation of the mean snow depths of the (six) manual transects at each site. Analysis indicated no meaningful relationship (R^2=0.12) between these measures of variability. Similarly, there is no meaningful relationship between inter-track variability and standard deviation of all manual points at a site.

3.1.3 Bulk density

Modeled and observed snow bulk densities are compared in the middle panel of Figure 6. Each modeled value is based on (1) the time series of snow depth estimated from GPS data at that site and (2) model parameters (Eqn. 1) and climatology of fit determined from neighboring SNOTEL sites. As shown in the P350 example (Figure 5), density is predicted for all days on which snow depth estimates exist. Only the modeled density from the day field data was collected is used for validation. Modeled and observed densities vary from 0.25 to 0.45 $g*cm^{-3}$ across the 16 density measurements, with the highest density values corresponding to the deepest snow. Model bias is effectively zero (<0.01 $g*cm^{-3}$) and RMSE is 0.04 $g*cm^{-3}$. This is equal to the RMSE for the

411 model applied to SNOTEL sites, using data around the time of peak SWE [*McCreight and Small*,
412 2014]. However the R^2 value (.53) is lower than found (.71) when the model is applied to
413 SNOTEL sites.

414 The two largest density errors were -.11 g*cm^{-3} at P019, though GPS-measured mean snow
415 depth was relatively accurate, and .05 g*cm^{-3} at P023. The density RMSE is dominated by these
416 two errors and excluding them halves the density RMSE to 0.02 g*cm^{-3}. In the discussion we
417 consider these large modeled density errors in more detail. Density errors of the remaining 14
418 observations are small and arise due to several factors, including measurement error, variability
419 of density at a site, and parameter transfer.

420 ***3.1.4 SWE***

421 The bottom panel of Figure 6 compares *in situ* and GPS-based SWE values. The GPS SWE data
422 accurately (R^2=.97) portray the observed variations across the 18 sites, from 0 to 60 cm SWE.
423 Bias and RMSE in SWE are essentially those of snow depth, scaled by the density. This indicates
424 that the SWE error is dominated by the depth error. Thus, the roughly -6 cm bias in depth
425 becomes a -2 cm bias for SWE, and the depth RMSE of 10.3 cm becomes 3.5 cm. Excluding
426 sites with less than 4 tracks available for calculating depth decreases these error statistics by
427 about 30%. These results show that the GPS reflections method yields SWE data at GPS sites
428 with errors that are small enough for most applications.

429 ***3.2 Time series observations***

430 In this section, we compare time series from GPS and *in situ* observations at three sites. This
431 comparison is intended to supplement the peak-accumulation validation data described in
432 Section 3.1. RN86 was the only site where it was feasible to complete manual depth and density
433 observations multiple times per season. In 2012 and 2013, manual observations were completed

434 at RN86 approximately every 3 weeks between January and May. Only the observations with the
435 largest depth measurements from each year were included in the peak-accumulation validation
436 analysis above. Figure 7 (top row) shows the time series of GPS and manual snow depth
437 observations from RN86. GPS-derived snow depth closely matches observed depth throughout
438 the season, not only at peak accumulation. Over the two years, the GPS snow depth bias is -2 cm
439 and RMSE is 5.5 cm. The observed and modeled density time series are compared in the middle
440 row of Figure 7. As is the case for depth, modeled density is very similar to observed. Bias is -
441 0.01 $g*cm^{-3}$ and RMSE is 0.03 $g*cm^{-3}$.

442 The bottom row of Figure 7 compares SWE time series. Over the ten observations, SWE Bias is
443 -1.5 cm and RMSE is 3.2 cm. GPS-based SWE underestimated the first two manual observations
444 in 2012 because both the GPS snow depth and the GPS-modeled density were underestimated.
445 By mid-March 2012, GPS SWE and *in situ* SWE are in closer agreement. The first manual
446 observation in 2013 is the only one in the 2 years that lies beyond one standard deviation of the
447 GPS-based estimate. The GPS-manual differences are much less during the remainder of 2013.
448 The three instances of SWE under-prediction demonstrate how even small depth errors can be
449 magnified by the density model. In general, depth underestimation will result in bulk density that
450 is too low, yielding an underestimation of SWE. The opposite occurs when depth is
451 overestimated. Therefore, if GPS snow depth is biased, it is reasonable to expect similar bias in
452 the modeled density and SWE products.

453 In Figure 8, we compare GPS snow depth time series to snow depth measured by time-lapse
454 photography at two PBO sites (P360 and P101) during the 2012 and 2013 water years. At P360,
455 GPS snow depth closely tracks the snow pole measurement throughout the season, including the
456 timing of accumulation and melt. On the day of the manual validation measurement (March

2012), depth at the snow pole and the GPS-derived depth are equal and approximately 10 cm below the site-average snow depth. At P101, the fluctuations in depth associated with accumulation and melt are again similar between the GPS and time-lapse data, but there are substantial differences in magnitude. Differences between the GPS snow depth and the time-lapse measurement change sign between the 2012 and 2013 water years. This was likely caused by the relocation of the snow pole during the intervening summer. On the date of manual measurement (March 2012), GPS-derived depth was nearly identical to site-averaged depth (Table 1, Figure 8), whereas depth at the snow pole was more than 10 cm lower. The large bias, both positive and negative, of a point measurement within the GPS footprint at P101 underscores the need for representative areal measurements to appropriately validate the GPS method. Comparison of these measurements highlights the utility of the large GPS sampling footprint, compared to data from other automated methods that sample at a scale of ~1 m^2.

4. Discussion

4.1 Sources of error in GPS-based depth and density

The validation data demonstrate that snow depth, density, and SWE estimated at PBO H2O GPS sites are accurate. At most sites, depth errors are less than 5 cm and SWE errors are less than 2 cm. Similarly, density errors in most cases are less than 0.02 $g*cm^{-3}$, small compared to errors associated with measuring density in snow pits. Some portion of the observed errors is likely the result of differences in how the manual and GPS data represent an average of the ~1000 m^2 area around the antenna. For example, the manual depth transects do not coincide exactly with the GPS ground tracks (Figure 4), especially at sites with few usable tracks. We now discuss other possible sources of depth and density errors that are revealed by the validation data described

above. Sources of SWE errors are not discussed separately, given the direct dependence of SWE on the other two variables.

A small negative bias is the most consistent feature of the GPS snow depth errors. The validation data show that GPS snow depth tends to be ~5 cm less than the average from manual observations. Excluding the four sites with less than four usable tracks, which undersample the GPS footprint, reduces the bias from -6 cm to -3 cm. This negative bias in the GPS depth estimates can be explained by two different factors, both of which may have affected our results. First, some portion of the received GPS signal is reflected from below the snow surface, either from within the snowpack or the underlying soil. These reflections will result in an underestimation of snow depth. This type of error is greatest when there is fresh, low-density snow at the surface, which reduces the permittivity contrast of the air-snow interface. Second, the bare ground surface used to estimate GPS snow depth may be several centimeters higher (relative to the antenna) than the ground surface sensed by the manual snow probe. The former is determined at each site based on reflection data from before and after the snow season. The manual probe may penetrate further into the vegetation litter and surface soil than this apparent reflection surface, yielding a negative bias in GPS snow depth.

Application of the *McCreight and Small* [2014] density model to H2O PBO sites was successful. The negative bias in GPS snow depth observations was small enough so that effects on density estimates were negligible. In addition, estimation of model parameters using depth and density measurements from SNOTEL sites did not obviously degrade density errors relative to the estimated errors. On average, GPS sites are ~400 m lower than the SNOTEL sites within 70 km that are used to identify model. In addition, many SNOTEL sites tend to be in small clearings within forests whereas the GPS sites in PBO H2O are situated in more exposed areas. Even with

these physiographic differences, errors reported here were nearly identical to those calculated for application of the model to SNOTEL sites [*McCreight and Small*, 2014]. This suggests that the model parameters are robust at the ~100 km scale for applications at peak accumulation, even given significant differences in elevation and vegetation.

Though the density model is not a great source of error, examination of the largest density errors provides some insight into its application. Fourteen of sixteen modeled density estimates were very accurate, together yielding an RMSE of 0.02 $g*cm^{-3}$. The model overestimated density at P023 by 0.05 $g*cm^{-3}$, an error similar in magnitude to errors associated with measuring density in snow pits. Therefore, it is difficult to learn anything conclusive about model performance from the overestimation at P023. In contrast, the error was much larger at P019 and warrants investigation. The modeled density was 0.33 $g*cm^{-3}$ and the observed density was 0.44 $g*cm^{-3}$, which was the highest value observed at all of the sites. Two factors likely contributed to the model underestimation. First, it was raining at P019 while the *in situ* data were being collected. This rainfall event increased density by ~0.04 $g*cm^{-3}$ over a two-day interval at a SNOTEL site ~5 km away and at similar elevation. The rainfall likely had a similar effect on density at P019. The model does not include rainfall as an input, and thus predicted density did not increase during this event. The second factor contributing to the error was that the snowpack was far below average in 2012. There had been little accumulation during the 2 months prior to the date of manual observation, which is very abnormal for this site. As a result, densification of the snowpack likely progressed more rapidly than in a typical year. Densities of .44 $g*cm^{-3}$, observed in mid-March in 2012, do not appear in the density climatology of fit for P019 until mid-May, just before melt out.

4.2 Are the validation data representative of conditions in the PBO H2O network?

525 The accuracy of GPS-based depth, density, and SWE was established using data from 18 PBO
526 H2O sites. The results presented above only constrain the network-wide errors if the validation
527 sites are representative of the ~130 snow sites throughout the network (Figure 1). The primary
528 factor to consider when comparing the sites used for validation and snow sites in the network is
529 the number of usable ground tracks. Our results show that the number of usable ground tracks
530 affects the accuracy of site-averaged snow depth estimates, and therefore estimates of SWE. The
531 number of usable tracks was considered when the validation sites were chosen. However, it was
532 of secondary importance in site selection relative to issues associated with site access and
533 location relative to other validation sites. The distribution of usable ground tracks is similar
534 between the subset of sites used for validation and the full network (Figure 9). Above, we
535 showed that sites with four or more usable ground tracks tend to produce accurate snow depth
536 estimates. GPS observations are based on four or more usable tracks 71% of the time in the H2O
537 PBO network and 80% of the time for the subset used for validation. Observations are based on
538 five or more tracks with almost identical frequency (59%) in the two distributions.

539 Other factors need to be considered when evaluating if the errors estimated from the validation
540 survey data are representative of PBO H2O. We quantified GPS snow depth errors around the
541 time of peak-accumulation. Snow depth errors did not depend on the magnitude of the snow
542 depth observations, so the peak-accumulation errors are likely representative of errors throughout
543 the snow season. This is supported by time series comparison at RN86 (Figure 7). In contrast,
544 density errors should be smallest at peak accumulation. *McCreight and Small* [2014] showed that
545 the density model errors were greatest at the beginning and end of the snow season, based on an
546 analysis of SNOTEL data. However, this probably has a limited effect on SWE errors for two
547 reasons. First, the density errors were mostly very small. Second, SWE errors are dominated by

548 snow depth errors. We expect that the SWE errors reported here are representative of those over
549 all PBO H2O network observations. Additional validation data would be useful to more
550 completely describe SWE errors throughout the snow season.

551 Based on this comparison and the results presented above, we conclude the following about the
552 accuracy of snow depth and SWE estimates at PBO H2O sites. First, the validation data provides
553 a representative description of errors at snow sites throughout the PBO H2O network. Second,
554 snow depth and SWE estimates are more reliable when many ground tracks are used at a site.
555 Four or more usable tracks are available for 71% of PBO H2O snow depth observations, which
556 yield more accurate estimates. Snow depth estimated at sites with one to three usable tracks
557 (~30% of PBO H2O snow sites) may closely match the average depth across the ~1000 m^2
558 footprint (e.g., P023 in Table 1). However, there is no way to confirm that this is the case
559 without continuous site visits. Thus, snow depth and SWE estimates from these sites should be
560 considered to have more uncertainty.

561 ***4.3 Considerations for future installations of GPS antennas to measure snow depth***

562 With the exception of RN86, all the sites used in this study were installed to study tectonic plate
563 boundary deformation, not for measuring snow depth. The selection of new sites for measuring
564 snow depth using reflected GPS signals should consider several constraints. GPS-based estimates
565 of snow depth are most reliable when many ground tracks are usable and spatial variability of
566 snow depth is not extreme. Terrain and vegetation around the antenna are the primary controls on
567 the number of ground tracks that yield usable data. Sites with extensive bedrock outcrops, slopes
568 greater than ~10 degrees, or otherwise complex topography should be excluded. Tall vegetation
569 obstructs the GPS signal, making some ground tracks unusable (see discussion and examples in
570 *Larson and Nievinski* [2013]). For example, tracks to the northwest and east of RN86 are

571 unusable due to trees (Figure 4). In most cases, problematic terrain and vegetation can be
572 identified from digital elevation models (DEMs) and Google Earth images. Terrain and
573 vegetation also affect the spatial variability of snow. Studies suggest that patterns of snow depth
574 spatial variability are relatively stable on interannual timescales (e.g. *Deems et al.* [2008]).
575 Therefore, it might be worthwhile to survey snow depth at candidate sites in the winter before
576 GPS installation to quantify snow depth variability.

577 The infrastructure used at GPS sites in general (and PBO in particular) was not designed for
578 sensing snow depth and could be improved for future installations. For example, many PBO
579 antennas are installed approximately 2m above the ground surface. Mounting antennas higher
580 above the surface (e.g., at 3 m) would be beneficial for snow sensing in two ways. First, a higher
581 antenna increases the size of the GPS measurement footprint. Second, a higher antenna would
582 limit the instances when the antenna is not at least two wavelengths above the snow surface.
583 Manual data were collected at P351, but the snow surface was nearly at the antenna height, so
584 GPS snow depth data available for comparison was known to be inaccurate. If the validation data
585 had been collected in a normal snow year, data from several other sites may have been similarly
586 affected. Raising the antenna in snowy regions would also benefit geophysicists – who currently
587 must throw out all data when the antenna has been covered with snow. This has been a particular
588 problem in Alaska, where many of the PBO sites were set at 1.5 meters above bare soil and are
589 regularly covered by snow each winter.

590 Antennas used by geodesists were designed to some extent to suppress reflections and thus are
591 not optimal for sensing snow depth. These GPS systems are also relatively expensive (more than
592 $5K per unit at the non-profit, group purchase price). If the only purpose of the instrument was
593 to measure snow depth, a cheaper instrument could be designed and deployed for snow sensing.

However, given the costs of maintaining the instrumentation in any network and the cost of data telemetry, combining the geodetic networks with snow sensing has significant advantages.

4.4 Applications of GPS-based snow products.

GPS-based snow depth, density, and SWE from GPS sites can be used in a similar fashion to data streams from other snow observing networks. PBO H2O snow products could be used to guide water resource management in snow-dominated watersheds. The near real-time GPS snow products, including error estimates, are updated daily (http://xenon.colorado.edu/portal). These allow the timing and rate of melt to be monitored with sufficient frequency for most applications. Another straightforward use of PBO H2O snow data is to provide ground-truth of remotely-sensed or modeled products. The relatively large sampling footprint of the GPS reflections data is advantageous in this application, compared to point or ~1 m^2 measurements.

PBO H2O sites complement sites in the SNOTEL network. Sites in both networks are distributed throughout the western US. However, the PBO H2O sites have very different physiographic conditions than most SNOTEL sites. First, SNOTEL sites are typically located in small clearings within forests and provide information about snowpack protected by forest canopies. In contrast, PBO H2O sites are necessarily located in either very large clearings, adjacent to forested areas (Figures 2a and 2b), or in non-forested ecosystems (Figure 2c). Thus, the effects of vegetation on snow accumulation and melt are different at PBO H2O and SNOTEL sites. Second, GPS snow sites are typically at lower elevations (440 m lower, on average) than neighboring SNOTEL sites. The combined effects of lower elevation and less vegetation result in shallower snow at many PBO H2O sites, compared to SNOTEL sites within the same region. Thus, the PBO H2O snow products provide a novel set of data. These data may be useful for improving assimilated

616 snow products (e.g., SNODAS) which may be biased in physiographic regions underrepresented
617 by current observing networks [*Clow et al.*, 2012].

618 **5. Conclusions**

619 Snow products derived from GPS reflections data closely match snow depth, density, and SWE
620 measured *in situ* at 18 PBO H2O sites. The validation comparison was completed around the
621 time of peak accumulation. Daily snow depth derived from GPS is very similar to mean snow
622 depth measured within a 25 m radius of the antenna, or at the ~1000 m^2 scale. There is a small
623 negative bias (-6 cm) that is consistent across the range of snow depths measured, from no snow
624 to 150 cm. The number of usable GPS ground tracks affects the error: when daily mean snow
625 depth is computed using four or more tracks, the snow depth bias is only -3 cm. Modeled snow
626 bulk density, based on GPS snow depth time series, closely matched density measured in a single
627 snow pit at each validation site. In 12 of 16 cases, density errors were less than 0.02 $g*cm^{-3}$.
628 Combining GPS-based depth and density yields an accurate estimate of SWE over its observed
629 range, from 0 to 60 cm (R^2 = 0.97 and bias = -2 cm). These results show that the near real time
630 PBO H2O snow products have errors small enough for most applications.

631 **Acknowledgements**

632 Data used in this paper are provided in Table 1 and are available online at:
633 *http://xenon.colorado.edu/portal/*.

634 This research was funded by NSF (EAR-0948957, AGS-0935725, EAR-1144221) and NASA
635 (NNH09ZDA001N, NNX11AL50H, NNX12AK21G, and NNH10ZDA001N). Some data,
636 equipment, and engineering services were provided by the Plate Boundary Observatory
637 (http://pbo.unavco.org) operated by UNAVCO for EarthScope and supported by NSF (EAR-
638 0350028 and EAR-0732947). We thank Jeffry Buechler for collecting snow depth and density

639 data. We thank Jobie Carlisle and the T.W. Daniel Experimental Forest of Utah State University
640 for measurements at the RN86 sites and for hosting the GPS antenna and Jim Normandeau for
641 setting up the time-lapse cameras. Felipe Nievinski and Praveen Vikram helped with many
642 technical issues. The free and open-source R software [*R Development Core Team*, 2011], along
643 with the reshape2, ggplot2, plyr, and scales packages [*Wickham,* 2007, 2009, 2011], were used
644 for analysis and presentation.

645 **References**

646 Beniston, M. (2003), Climatic change in mountain regions: a review of possible impacts,
647 In *Climate Variability and Change in High Elevation Regions: Past, Present & Future*, pp.
648 5-31, Springer, Netherlands.

649 Brazenec, W. A. (2005), Evaluation of ultrasonic snow depth sensors for automated surface
650 observing systems (ASOS), PhD diss., Colorado State University.

651 Cayan, D. R. (1996), Interannual climate variability and snowpack in the western United States,
652 *Journal of Climate, 9*(5), 928-948.

653 Cohen, J., and D. Entekhabi (1999), Eurasian snow cover variability and Northern Hemisphere
654 climate predictability, *Geophysical Research Letters*, *26*(3), 345-348.

655 Deems, J. S., S. R. Fassnacht, and K. J. Elder (2008), Interannual Consistency in Fractal Snow
656 Depth Patterns at Two Colorado Mountain Sites, *Journal of hydrometeorology* 9(5), 977-988.

657 Dickinson, W. T., and H. R. Whiteley (1972), A sampling scheme for shallow
658 snowpacks, *Hydrological Sciences Journal*, *17*(3), 247-258.

659 Dietz, A. J., C. Kuenzer, U. Gessner, and S. Dech (2012), Remote sensing of snow–a review of
660 available methods, *International Journal of Remote Sensing*, *33*(13), 4094-4134.

661 Dixon, D. and Boon, S. (2012), Comparison of the SnowHydro snow sampler with existing snow
662 tube designs, *Hydrolgic Processes*, *26*, 2555–2562, doi: 10.1002/hyp.9317

663 Elder, K. J., J. Dozier, and J. Michaelsen (1991), Snow accumulation and distribution in an
664 alpine watershed, *Water Resources Research*, *27*(7), 1541-1552.

665 Elder, K. J., W. Rosenthal, and R. E. Davis (1998), Estimating the spatial distribution of snow
666 water equivalence in a montane watershed, *Hydrological Processes*, *12*(1011), 1793-1808.

667 Farnes, P. E., B. E. Goodison, N. R. Peterson, and R. P. Richards (1983), Final Report,
668 Metrication of Manual Snow Sampling Equipment, Western Snow Conference, Spokane,

669 Washington, http://www.westernsnowconference.org/sites/
670 westernsnowconference.org/PDFs/1982Farnes.pdf

671 Garvelmann, J., S. Pohl, and M. Weiler (2013), From observation to the quantification of snow
672 processes with a time-lapse camera network, *Hydrology and Earth System Sciences*, *17*,
673 1415–1429, doi:10.5194/hess-17-1415-2013, 2013.

674 Goodison, B. E., J. E. Glynn, K. D. Harvey, and J. E. Slater (1987), Snow surveying in Canada: a
675 perspective, *Canadian Water Resources Journal*, *12*(2), 27-42.

676 Gutmann, E. D., K. M. Larson, M. W. Williams, F. G. Nievinski, and V. Zavorotny (2012),
677 Snow measurement by GPS interferometric reflectometry: an evaluation at Niwot Ridge,
678 Colorado, *Hydrological* Processes, *26*(19), 2951-2961.

679 Harpold, A. A., Q. Guo, N. Molotch, P. D. Brooks, R. Bales, J. C. Fernandez-Diaz, K.
680 N. Musselman, T. L. Swetnam, P. Kirchner, M. Meadows, J. Flannagan, and R. Lucas
681 (2014), A LiDAR derived snowpack dataset from mixed conifer forests in the Western U.S.,
682 *Water Resources Research*, doi: 10.1002/2013WR013935, in press.

683 Johnson, J. B., A. Gelvin, and G. Schaefer (2007), An engineering design study of electronic
684 snow water equivalent sensor performance, In *75th annual Western snow conference,*
685 *Kailua-Kona, Hawaii*,16-19.
686 (http://www.westernsnowconference.org/sites/westernsnowconference.org/PDFs/2007Johnso
687 n.pdf)

688 Larson, K. M., and F. G. Nievinski (2013), GPS snow sensing: results from the EarthScope Plate
689 Boundary Observatory, *GPS solutions*, *17*(1), 41-52.

690 Larson, K. M., E. D. Gutmann, V. U. Zavorotny, J. J. Braun, M. W. Williams, and F. G.
691 Nievinski (2009), Can we measure snow depth with GPS receivers?, *Geophysical Research*
692 *Letters*, *36*(17).

693 Larson, K. M., E. E. Small, E. D. Gutmann, A. L. Bilich, J. J. Braun, and V. U. Zavorotny
694 (2008), Use of GPS receivers as a soil moisture network for water cycle studies, *Geophysical*
695 *Research Letters*, *35*(24).

696 Marchand, W., and A. Killingtveit (2004), Statistical properties of spatial snowcover in
697 mountainous catchments in Norway, *Nordic hydrology*, *35*(2), 101-117.

698 McCreight, J.L. and E. E. Small (2014), Modeling bulk density and snow water equivalent using
699 daily snow depth observations, *The* Cryosphere, http://www.the-cryosphere-
700 discuss.net/7/5007/2013/tcd-7-5007-2013.html), in press.

701 Nievinski, F.G. and K.M. Larson (2014a), Forward and Inverse Modeling of GPS Multipath for
702 Snow Depth Estimation, I: Formulation and Simulations, *IEEE TGRS,*
703 10.1109/TGRS.2013.2297681, (available at *http://xenon.colorado.edu/portal/*
704 *index.php?action=publications), in press.*

Nievinski, F.G. and K.M. Larson (2014b), Forward and Inverse Modeling of GPS Multipath for Snow Depth Estimation, II: Application and Validation, *IEEE TGRS,* 10.1109/TGRS.2013.2297688, *(available at http://xenon.colorado.edu/portal/index.php?action=publications), in press.*

Painter, T. H., K. Rittger, C. McKenzie, P. Slaughter, R. E. Davis, and J. Dozier (2009), Retrieval of subpixel snow covered area, grain size, and albedo from MODIS, *Remote Sensing of Environment*, *113*(4), 868-879.

Pomeroy, J. W. and Gray, D. M. (1995), Snow Accumulation, Relocation and Management, NHRI Science Report No.7. Supply and Services Canada, Saskatoon. 144 pp.

Press F, S. Teukolsky, W. Vetterling, B. Flannery (1996), Numerical recipes in Fortran 90: the Art of parallel scientific computing, 2nd edn. Cambridge University Press, Cambridge.

R Core Team (2012), R: A language and environment for statistical computing. R Foundation for Statistical Computing, Vienna, Austria. ISBN 3-900051-07-0, http://www.R-project.org/.

Rittger, K., T. H. Painter, and J. Dozier (2013), Assessment of methods for mapping snow cover from MODIS, *Advances in Water Resources*, *51*, 367-380.

Ryan, W. A., N. J. Doesken, and S. R. Fassnacht (2008), Evaluation of ultrasonic snow depth sensors for US snow measurements, *Journal of Atmospheric and Oceanic Technology*, *25*(5), 667-684.

Small, E. E., K. M. Larson, and J. J. Braun (2010), Sensing vegetation growth with reflected GPS signals, *Geophysical Research Letters*, *37*(12), L12401.

Serreze, M. C., Clark, M. P., Armstrong, R. L., McGinnis, D. A., and Pulwarty, R. S. (1999), Characteristics of the western United States snowpack from snowpack telemetry (SNOTEL) data, *Water Resources Research*, *35*(7), 2145–2160.

Stepphun, H. and G. E. Dyck (1974), Estimating the true basin snowcover, Advances Concepts and Techniques in the Study of Snow and Ice Resources, Asilomar Conference Grounds, Monterey, CA, USA, National Academy of Sciences, Washington, D.C..

Sturm, M. (2009), Field techniques for snow observations on sea ice, in *Field Techniques for Sea-Ice Research*, H. Eicken, R. Gradinge, M. Slaganek, K. Shirasawa, D. Perovich, M Lepparanta, pp25-48, University of Alaska Press, Fairbanks, AK.

Sturm, M., B. Taras, G. Liston, C. Derksen, T. Jonas, J. Lea (2010), Estimating snow water equivalent using snow depth data and climate classes, *Journal of Hydrometeorology*, 11(6), 1380–1394.

Walsh, J. E. (1984), Snow Cover and Atmospheric Variability: Changes in the snow covering the earth's surface affect both daily weather and long-term climate, *American Scientist*, *72*(1), 50-57.

Wickham, H. (2007), Reshaping Data with the reshape Package, *Journal of Statistical Software*, *21*(12), 1-20.

Wickham, H. (2009), *ggplot2: elegant graphics for data analysis*, Springer.

Wickham, H. (2011), The split-apply-combine strategy for data analysis, *Journal of Statistical Software*, *40*(1), 1-29.

Tables

Table 1. Near peak accumulation validation data[a]

site:		p019	p023[b]	p029[b]	p029	p030	p088	p101	p118	p350	p351	p353	p360	p455	p460	p676	p682	p683	p684	rn86	rn86
Year		2012	2012	2012	2013	2012	2012	2012	2012	2012	2012	2012	2012	2012	2012	2012	2012	2012	2012	2012	2013
Day of year		75	74	67	85	69	68	69	68	93	93	76	71	94	73	72	69	70	71	55	114
# of GPS Tracks		5	3, 2	4	5	8	4	9	9	3	4	7	12	5	4	3	1	6	10	6	7
Depth (cm)	GPS	39.9	71.2	67.9	67.2	0.0	10.5	27.3	29.5	138.8	131.4	0.0	75.0	66.7	9.8	41.4	41.1	47.0	0.0	143.9	138.0
	Transects	34.5	72.7	73.6	73.4	0.0	16.7	25.2	37.9	146.4	154.7	0.0	87.8	64.2	14.1	72.7	59.5	62.0	0.0	140.1	141.8
Stdev Depth (cm)	GPS	6.4	10.7	5.2	5.3	4.3	3.3	5.3	4.3	4.8	4.3	3.8	4.0	3.3	5.6	2.7	5.0	7.1	3.0	13.2	5.9
	Transects	1.3	1.0	6.8	5.2	0.0	5.5	8.7	7.9	5.3	12.9	0.0	5.8	32.6	5.2	27.4	7.4	5.9	0.0	3.2	1.5
	Points	5.0	4.7	10.9	10.4	0.0	12.1	14.9	9.5	7.1	20.9	0.0	9.0	33.5	12.1	31.4	18.9	8.7	0.0	4.6	4.7
Density ($g*cm^{-3}$)	GPS	0.33	0.33	0.26	0.30		0.27		0.25	0.35	0.36		0.27	0.29	0.26	0.27	0.29	0.27		0.28	0.42
	Pit	0.44	0.28	0.28	0.30		0.24		0.29	0.37	0.34		0.27	0.33	0.24	0.27	0.27	0.28		0.30	0.39
SWE (cm)	GPS	13.2	23.8	17.7	20.4	0.0	2.8		7.4	49.0	46.7	0.0	20.2	19.3	2.5	11.3	12.1	12.7	0.0	39.6	58.5
	Pit	15.0	20.3	20.9	22.2	0.0	4.0		10.9	54.4	52.6	0.0	24.0	21.1	3.4	19.4	16.2	17.5	0.0	42.6	55.3

[a]GPS snow depth is the mean calculated from all usable tracks. Standard deviation of *in situ* snow depth is calculated in two ways: (1) standard deviation of the transect-mean snow depths; and (2) the standard deviation over all manual point measurements. Density is not reported for sites with no snow.

[b]GPS values are interpolated from observations on adjacent days as no observations were available on the day of manual measurement. Number of GPS tracks is shown for both days.

.

Table 2. GPS snow depth and SWE statistics calculated four ways[a]

	Including snow-free obs	GPS footprint depends on snow depth	Bias (cm)	RMSE (cm)	R^2
Snow Depth (cm)			-6.7	11.3	0.95
	✓		-5.7	10.3	0.96
		✓	-6.2	10.3	0.96
	✓	✓	-5.2	9.5	0.97
SWE (cm)			-2.5	3.8	0.97
	✓		-2.0	3.5	0.97
		✓	-2.3	3.6	0.97
	✓	✓	-1.9	3.3	0.97

[a]The three sites with no observed snow on the day of the manual survey are either included (checked) or excluded. Manual observations from either the smaller, snow-depth-dependent footprint (checked) or the larger, snow-free GPS footprint are also compared.

Figures

Figure 1. PBO H20 sites used for validation of the GPS snow products are shown with pink triangles. All other PBO H2O sites are shown in blue. Other PBO GPS locations in the western, continental US are indicated with grey dots.

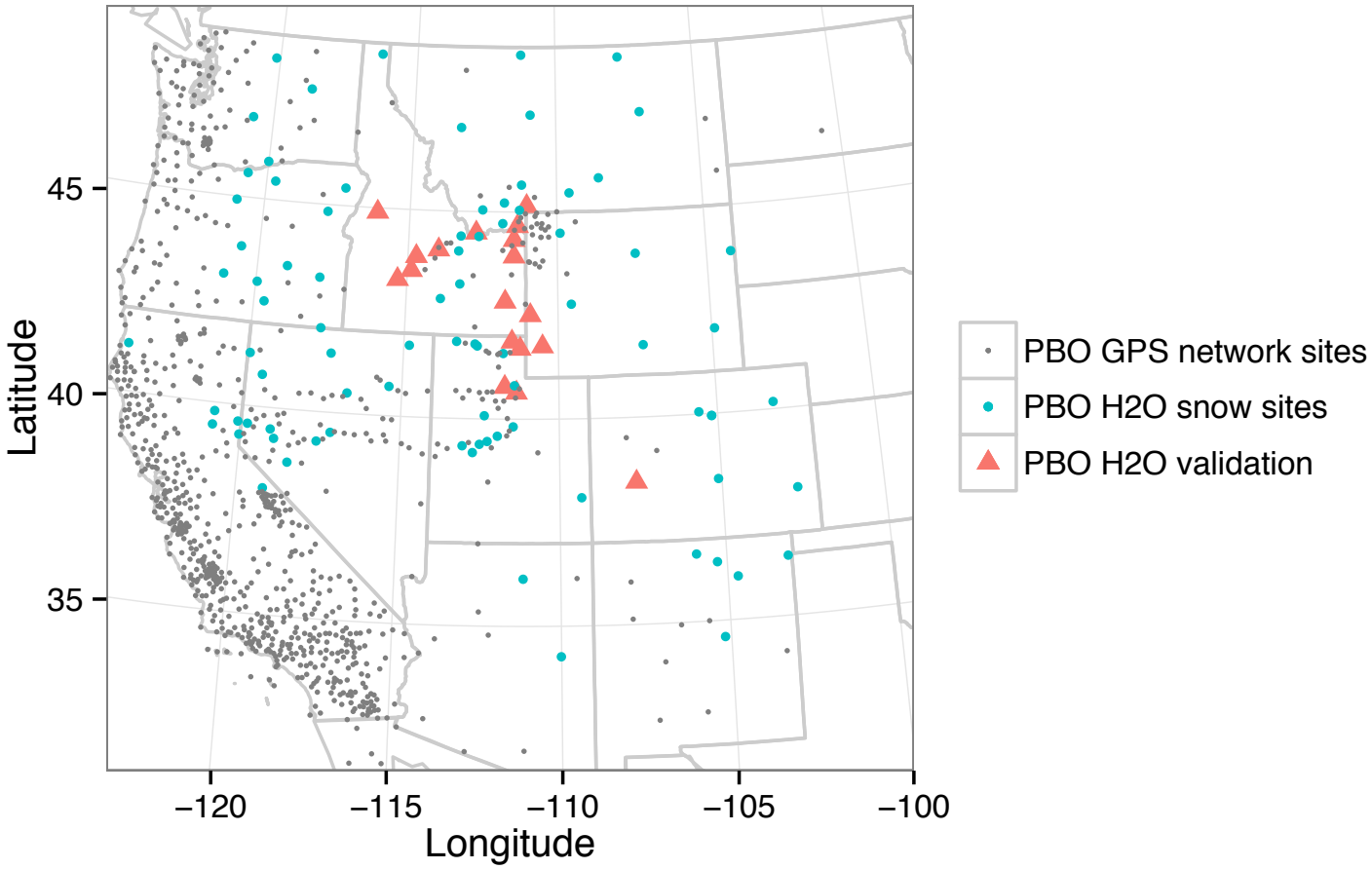

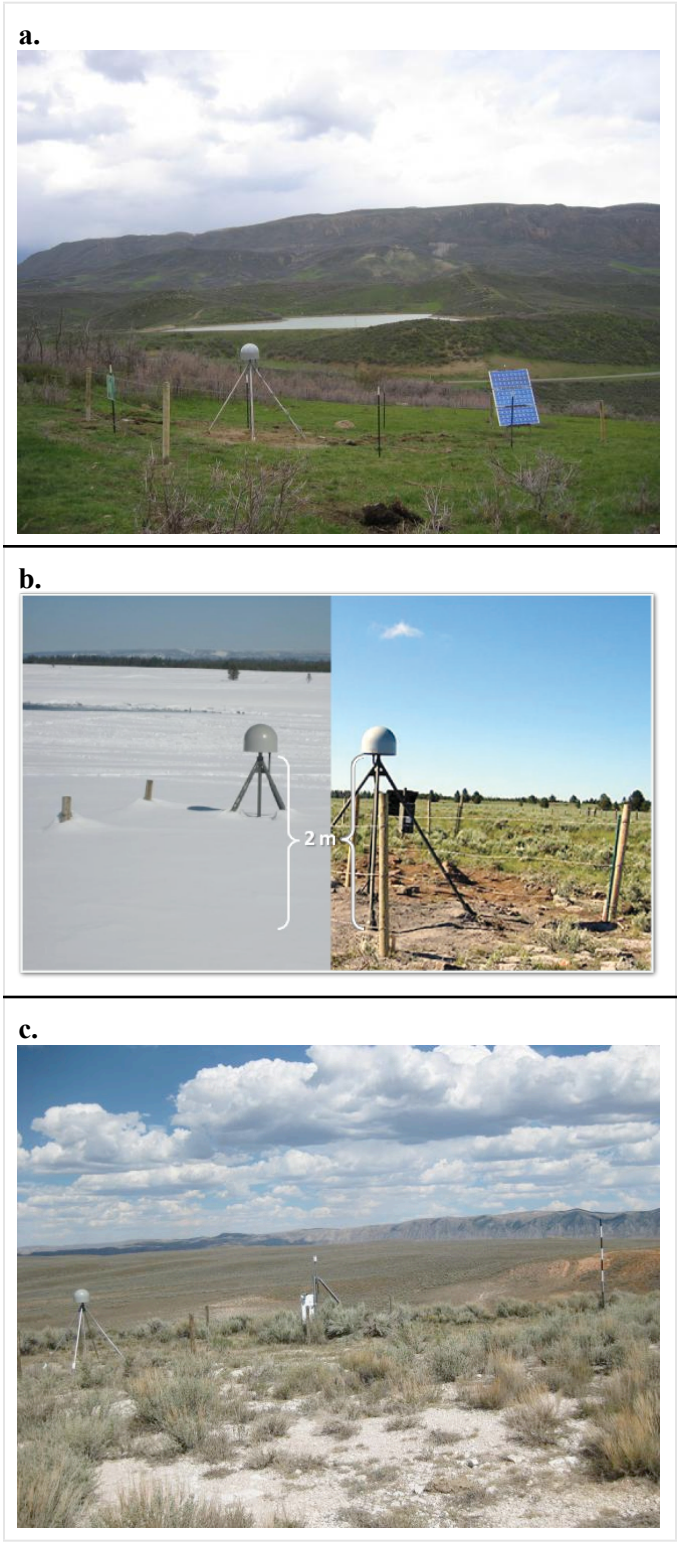

Figure 2. Example of three PBO GPS sites used for validation. **a.** P029, Colorado. **b.** P360, Idaho, with and without snow. **c.** P101, Utah. The black and white pole on the right of image is used for automated photography of snow depth within the GPS footprint.

Figure 3. GPS satellites transmit a signal that arrives on the Earth as a plane wave. The ground or snow surface acts as a planar reflector, shown in gray. The antenna is represented by the black circle. The direct signal (blue) travels a shorter distance to the antenna than the reflected signal (blue plus red). The extra path length depends on the elevation angle of the satellite with respect to the horizon, *e*. The GPS carrier signal (wavelength=24.4 cm) is shown superposed on the direct signal. Depending on the extra path travelled by the reflected signal, the interference between the direct and reflected signals varies (shown for three examples in the center of the figure). This interference (shown in black) is what is measured by the GPS unit in its Signal to Noise Ratio data.

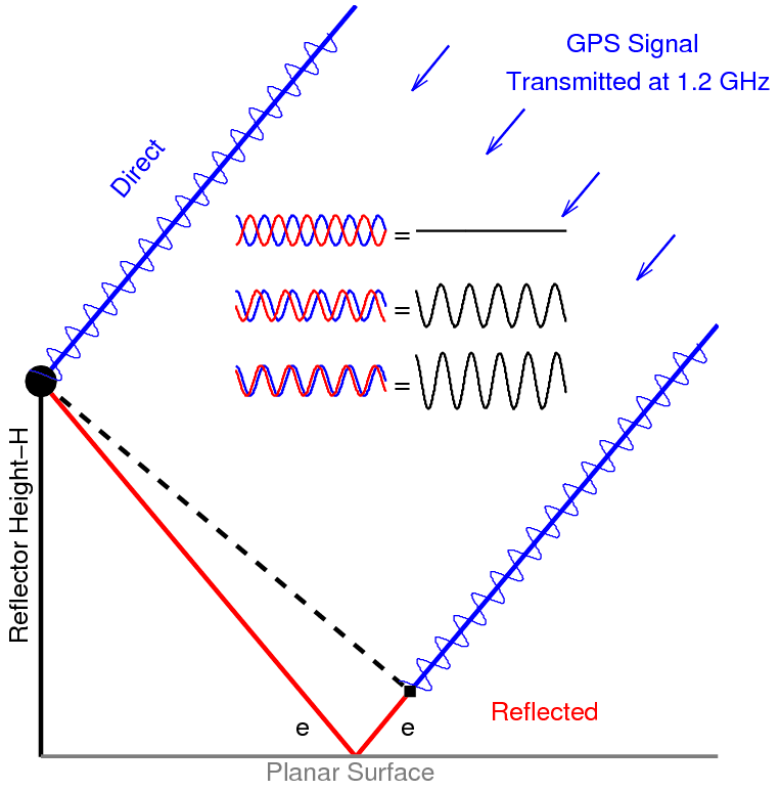

Figure 4. The spatial footprint of the GPS snow depth method is illustrated along with the location of manual observations collected for validation. The GPS footprint is comprised of ground tracks of individual GPS satellites, roughly indicated by different color ellipses. The ellipses actually represent the first Fresnel zones for satellites at 10 deg elevation angle and for a (snow-free) antenna height of 2m. The first Fresnel zone is the area of primary surface reflections. It shrinks in size and moves towards the antenna at greater elevation angles and for shorter antenna heights caused by snow accumulation. Only a subset of the GPS ground tracks produces acceptable data to estimate snow depth. The white points illustrate the manual snow depth sampling locations. The red dot indicates the approximate location of snow pits where density and SWE were measured for comparison against modeled values.

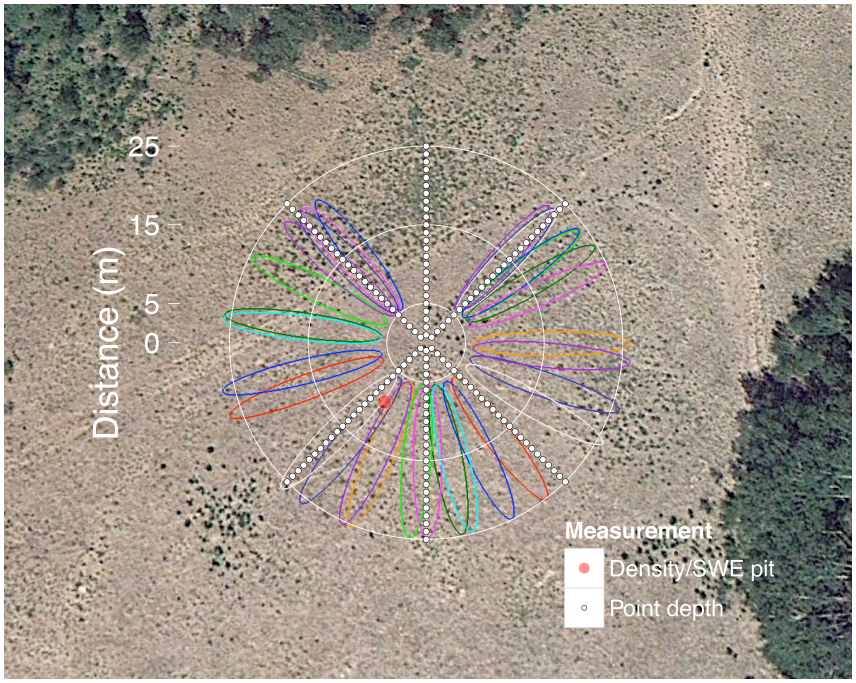

Figure 5. Example density and SWE calculation for site P350. All error bars represent ±1 standard deviation. **Panel 1**: GPS snow depth observations, the primary input to the density model. **Panels 2-4**: Model predictors; *hAvg* is computed using the GPS snow depth and a centered, 21-day window; Anomalies (*hAbove* and *hBelow*) of observed snow depth relative to *hAvg*; and daily climatology of fit, ρ*Clim*. **Panel 5**: Modeled bulk density. **Panel 6**: Estimated SWE. The red points overlaying the GPS estimates indicate the manual, validation measurements of depth, density, and SWE. The vertical red bar highlights the day of validation near peak snow accumulation.

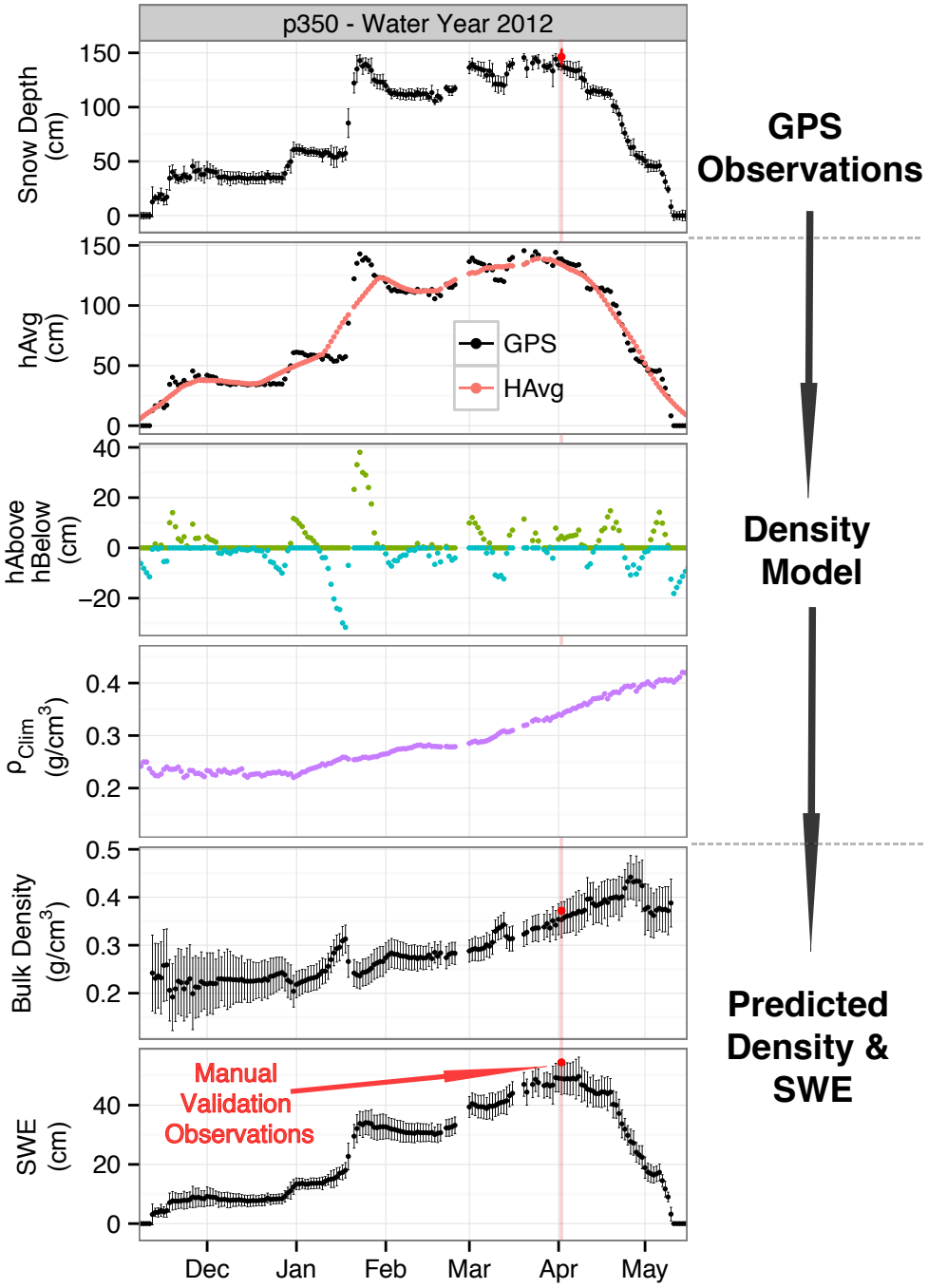

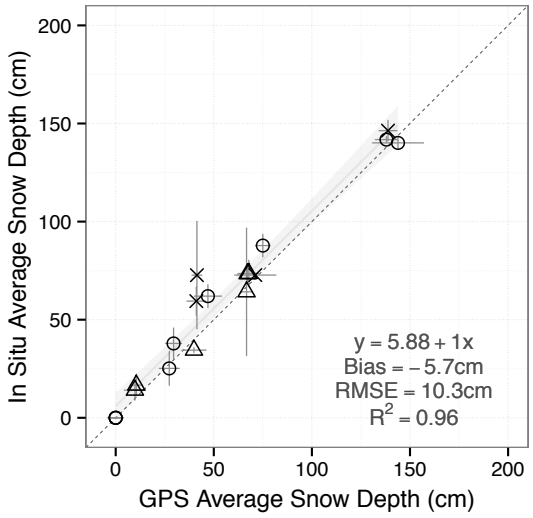

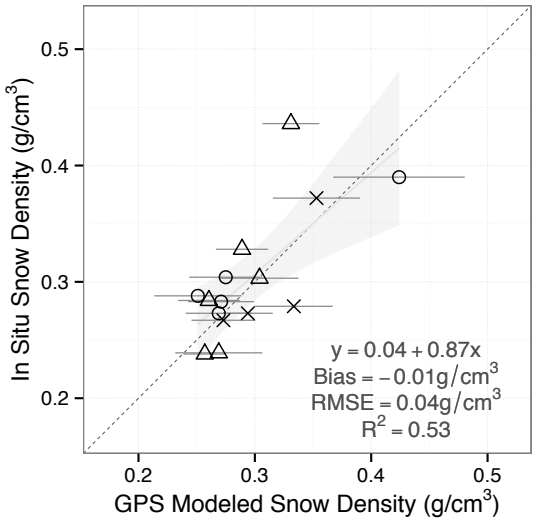

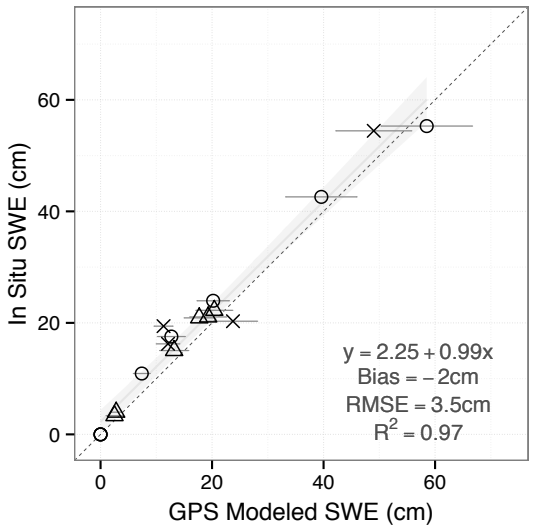

Figure 6. GPS versus manual snow depth, density, and SWE at 18 PBO H2O sites near peak accumulation. The individual values are presented in Table 1. Symbols indicate the number of ground tracks used to estimate depth: x is 1-3, circle is 4-5, and triangle is 6-12. Error bars represent 1 standard deviation. The 1-1 line is dashed. The regression relationship with standard error of fit is shown by a solid grey line and a shaded area. Coefficients of fit and statistics (including snow-free observations of depth and SWE) are shown in the plots.

Figure 7. The left and center columns show time series of GPS snow depth measurements, modeled density and SWE estimates at the RN86 site and manual measurement in red. Uncertainty is represented by +/- one-standard-deviation error bars. Error bars on the manual measurements represent the standard deviations over all snow depth points surveyed (not transect-mean snow depth). The right-hand column is a scatter plot of all corresponding GPS and manual observations at RN86 for each variable.

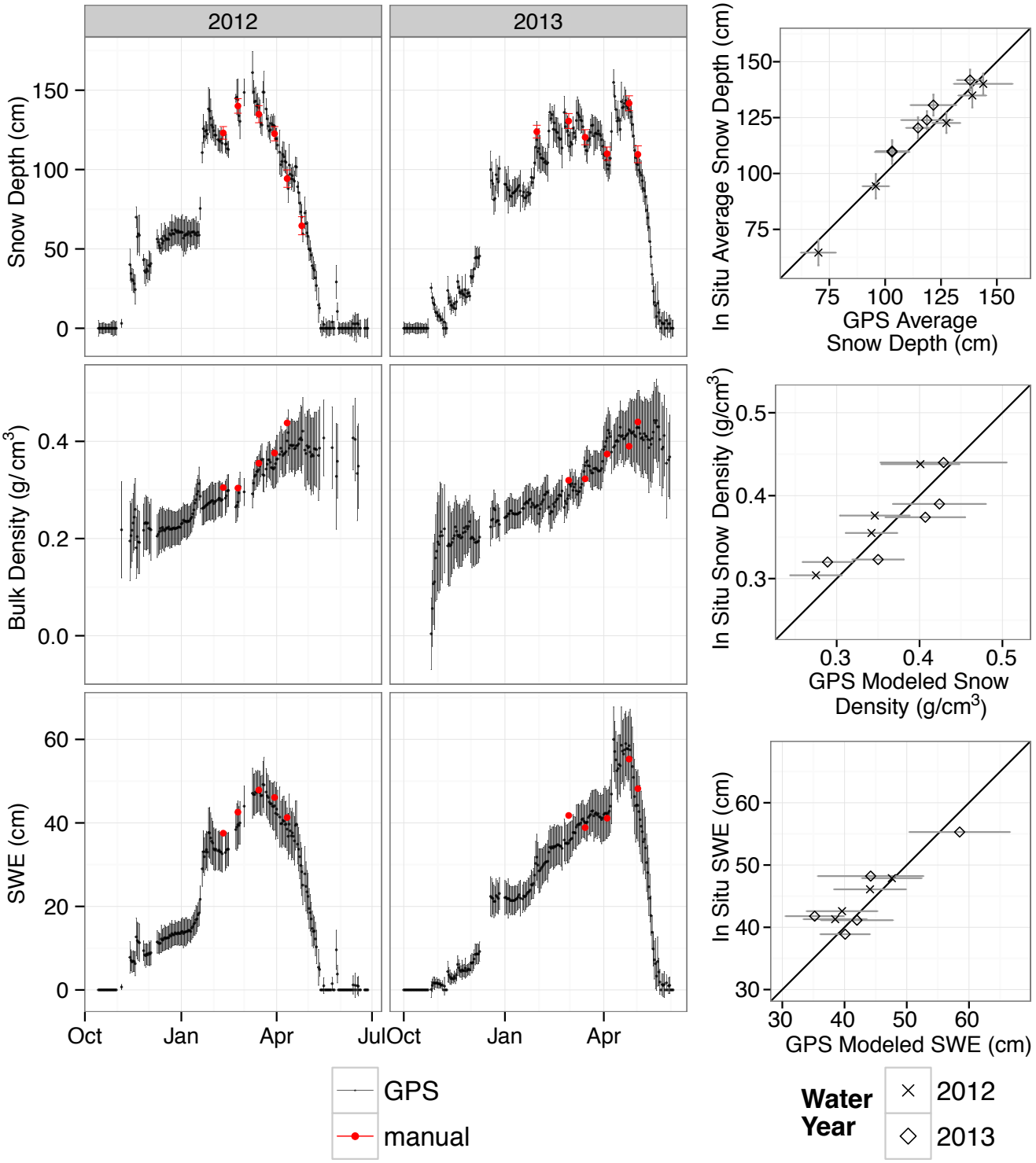

Figure 8. GPS (black), manual (red), and time-lapse snow pole (blue) snow depth measurements at P101 and P360. Manual observations were only made in 2012 at these sites. Error bars for GPS and manual measurements are the same as in Figure 7.

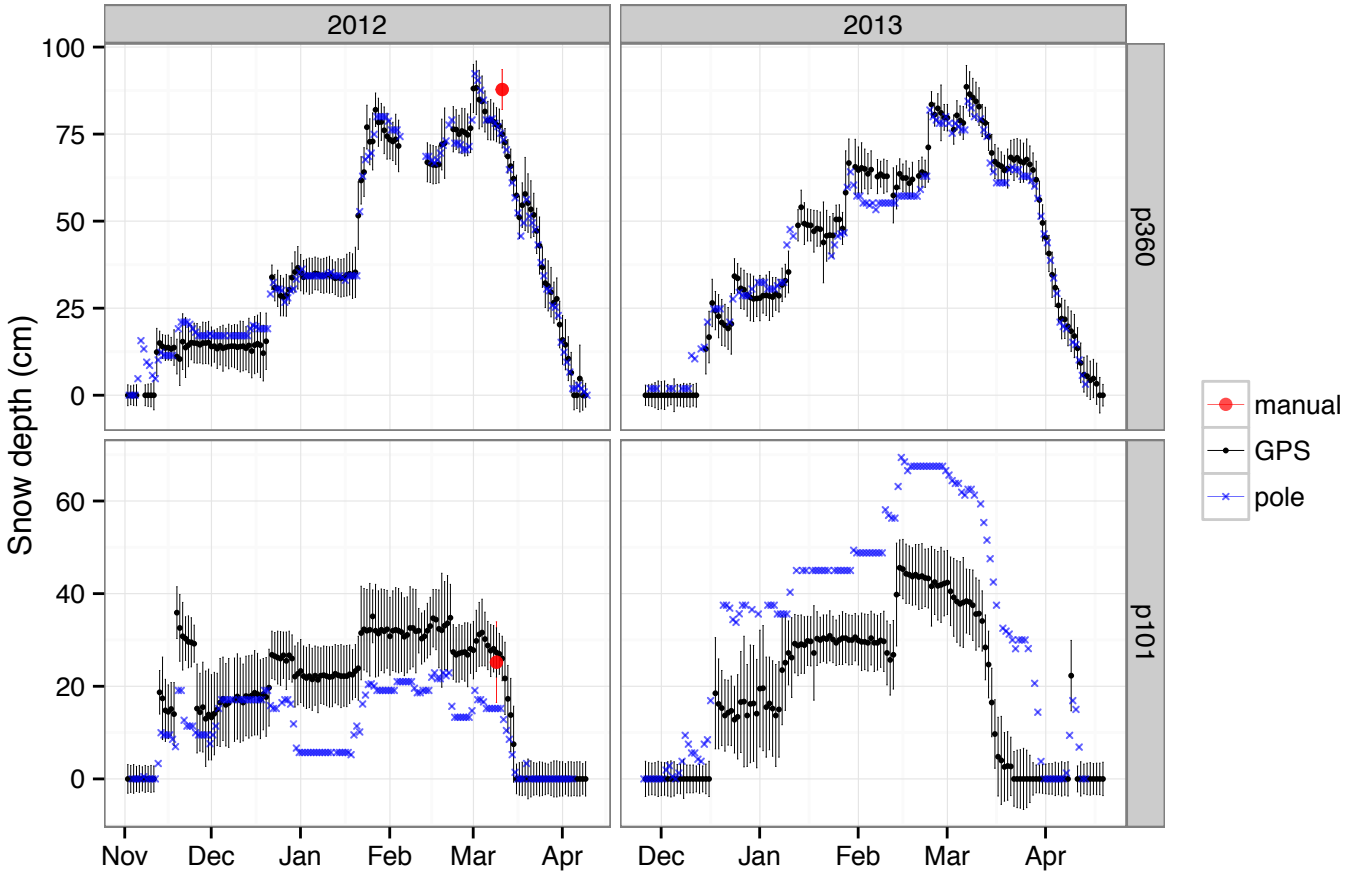

Figure 9. Distribution of the number of usable GPS ground tracks for snow depth estimates. The histogram and the y-axis correspond to the validation sites. The dashed line shows the distribution of usable GPS tracks for all PBO H2O depth measurements greater than 10cm (13,303 measurements at 130 sites), which is not scaled to y-axis (the mode is 3 GPS tracks with 2158 observations).